Fenton-like Chemistry in Water: Oxidation Catalysis by Fe(III) and H_2O_2

Bernd Ensing,[†] Francesco Buda,[‡] and Evert Jan Baerends*[,†]

Theoretical Chemistry, Faculty of Sciences, Vrije Universiteit Amsterdam, De Boelelaan 1083, 1081 HV Amsterdam, The Netherlands and Leiden Institute of Chemistry, Gorlaeus Laboratories, Leiden University, The Netherlands

Received: August 8, 2002; In Final Form: March 17, 2003

The formation of active intermediates from the Fenton-like reagent (a mixture of iron(III) ions and hydrogen peroxide) in aqueous solution has been investigated using static DFT calculations and Car−Parrinello molecular dynamics simulations. We show the spontaneous formation of the iron(III) hydroperoxo intermediate in a first step. The Fenton-like reaction thus proceeds very differently compared to Fenton's reagent (i.e., the Fe^{II}/H_2O_2 mixture), for which we have recently shown that the first step is the spontaneous O−O lysis of hydrogen peroxide when coordinated to iron(II) in water. For the second step in the reaction mechanism of the Fenton-like reagent, we compare the possibilities of homolysis and heterolysis of the O−O bond and the Fe−O bond of the produced $[(H_2O)_5Fe^{III}OOH]^{2+}$ intermediate. We find that concomitant hydrolysis of the reacting species plays a crucial role and, taking this into account, that O−O homolysis ($[(H_2O)_4(OH)Fe^{III}\text{-}OOH]^+ \rightarrow [(H_2O)_4(OH)Fe^{IV}O]^+ + OH^\bullet$) in vacuo is a likely second step with $\Delta E_{0k}^{\ddagger} = 26$ kcal/mol. However, proper inclusion of the solvent effects is important, in particular, for the heterolysis reactions, in which case the large endothermicy of the charge separations can be compensated by the hydration energies from the ion solvation. In this work, we also calculate the free energy barrier for the O−O homolysis of the iron(III) hydroperoxo intermediate in aqueous solution at $T = 300$ K, using the method of constrained molecular dynamics and thermodynamic integration, resulting in $\Delta A_{300K}^{\ddagger} = 21$ kcal/mol. Analysis of the vibrational spectra of the high-spin ($S = 5/2$) and low-spin ($S = 1/2$) Fe(III)OOH intermediates confirm the, in the literature, suggested effect of the spin state on the Fe−O and O−O bond strengths. In fact, we predict that with ligands inducing a low-spin iron(III) hydroperoxo intermediate, the barrier for the O−O homolysis will be even significantly lower.

I. Introduction

The activation of oxygen by transition-metal oxides is of fundamental importance in organic synthesis, catalysis, and biochemistry. Efficient catalysts are found in nature for the hydroxylation and oxidation of organic molecules. Examples are cytochrome P450, methane monooxygenase (MMO), and the antitumor drug bleomycin (BLC), all of which have low-valent iron ions as the active centers that can be turned into highly reactive high-valent iron−oxo, iron−peroxo, or iron−hydroperoxo complexes. Also, Fenton's reagent, a mixture of iron(II) ions and hydrogen peroxide, is widely applied to oxidize organic substrates. Although H. J. H. Fenton himself used the unchelated Fe^{2+}/H_2O_2 mixture in acidic aqueous solution when he first recorded the oxidative potential of this mixture in 1876,[1,2] many modifications have since been applied in order to alter the reactivity, to enhance the solubility in other solvents, to increase the pH range, and to avoid precipitation of the metal catalyst. This has led to a great variety of ligated iron(II) complexes in combination with H_2O_2 (or HOCl) or even with different transition metals, such as Mn(II) or Fe(III), which are all often referred to as *Fenton's reagent*. To distinguish between the iron(II) and iron(III) combinations, we will, however, follow the convention of using *Fenton-like reagent* for the Fe^{3+}/H_2O_2 mixture and restrict the use of *Fenton's reagent* to denote the Fe^{2+}/H_2O_2 mixture. The Fenton-like reagent is also capable of oxidizing organic substrates, but it is somewhat less reactive than Fenton's reagent. As iron(III) can be produced in applications of Fenton's reagent, Fenton chemistry and Fenton-like chemistry often occur simultaneously. Interestingly, Fenton and Fenton-like chemistry are generally believed to proceed via similar mechanisms as oxidation reactions with the aforementioned complex and bulky enzymes.

Until recently, Fenton chemistry was still far from being fully understood. Numerous reaction mechanisms have been proposed based on different active intermediates such as OH• and OOH• radicals and the earlier mentioned high-valent iron species. Haber and Weiss' OH• radical mechanism[3] is probably the most popular candidate for the Fenton reaction

$$Fe^{2+} + H_2O_2 \rightarrow Fe^{3+} + OH^- + OH\bullet \qquad (1)$$

followed by the alternative mechanism first suggested by Bray and Gorin,[4] in which the ferryl ion, $[Fe^{IV}O]^{2+}$, is supposed to be the active intermediate

$$Fe^{2+} + H_2O_2 \rightarrow [Fe^{IV}O]^{2+} + H_2O \qquad (2)$$

In both mechanisms, the hydrogen peroxide O−O lysis forms the essential step. We have recently performed static density functional theory (DFT) calculations to study the active species produced by hydrated Fenton's reagent $[Fe^{II}(H_2O)_5(H_2O_2)]^{2+}$ in vacuo[5] as well as ab initio (DFT) molecular dynamics (AIMD) simulations of Fe^{2+} and H_2O_2 in aqueous solution.[6,7]

[†] Vrije Universiteit Amsterdam.
[‡] Leiden University.

10.1021/jp0267149 CCC: $25.00
Published on Web 07/09/2003

In this work, we showed that the ferryl ion is easily formed when hydrogen peroxide coordinates to an iron(II) ion in water, which confirms the reaction mechanism first proposed by Bray and Gorin (eq 2). Moreover, formation of the ferryl ion from hydrated Fenton's reagent in vacuo was found to be energetically favored over the formation of free hydroxyl radicals (eq 2).

For the Fenton-like reagents, it is believed that initially no O−O bond breaking takes place, but instead an iron(III) hydroperoxo intermediate is formed as the first step via hydrolysis

$$Fe^{3+} + H_2O_2 \rightarrow [Fe^{III}OOH]^{2+} + H^+ \quad (3)$$

This intermediate might be able to react with organic substrates or break up in smaller active species in a second step. The iron(III) hydroperoxo may, e.g., homolyze at the Fe−O bond[8−10]

$$[Fe^{III}OOH]^{2+} \rightarrow Fe^{2+} + OOH\bullet \quad (4)$$

generating iron(II) and producing the reactive OOH• radical or at the O−O bond producing the ferryl ion and an OH• radical[10,11]

$$[Fe^{III}OOH]^{2+} \rightarrow [Fe^{IV}O]^{2+} + OH\bullet \quad (5)$$

Alternatively, O−O bond heterolysis could take place, producing the highly reactive Fe^V species[10,12]

$$[Fe^{III}OOH]^{2+} \rightarrow [Fe^{V}O]^{3+} + OH^- \quad (6)$$

Probably many of the proposed mechanisms compete with each other depending on the reaction conditions, such as the metal ligands, the solvent, the pH, and the organic substrate to be oxidized. This is, of course, one of the reasons why Fenton-like chemistry still holds secrets. Another important reason is the very elusive nature of the active species, which live too short to have been definitively observed yet in experiments. Obviously, that is not a problem for computer simulations.

In the present work, we will investigate the active species for the Fenton-like chemistry and focus on the differences between iron(II) and iron(III) in activating hydrogen peroxide. To simulate the generation, evolution, and termination of reactive intermediates such as hydroxyl radicals we need an accurate description of the aqueous environment. The method of choice is ab initio (DFT) molecular dynamics method (AIMD), using the Car−Parrinello technique, which has already proven to be a very useful tool for our type of systems.[6,13−15] Density functional theory (DFT) has already proven to be very useful for the unraveling of the activation mechanisms of MMO[16−21] and P450[22−26] and the oxidation of methane and benzene with the bare ferryl ion (Fe^{IV}═O).[27−33]

This paper is organized as follows. First, we briefly summarize the computational details in section 2. In section 3, we present our results, starting with the static DFT calculations of the energetics of the proposed elementary Fenton and Fenton-like reactions of the hydrated iron hydrogen peroxide complexes in vacuo. Clearly, the different nature of the Fe(III)/H_2O_2 reagent compared to the Fe(II)/H_2O_2 reagent is revealed, showing that OH• radical or ferryl ion formation via O−O lysis as the first mechanistic step is energetically very unfavorable and instead hydrolysis (eq 3) is indeed predicted to be the most likely initial step. However, realistic modeling of the hydrolysis, i.e., simulating the donation of H^+ by the iron(III) complex to the aqueous solution, requires the explicit inclusion of the solvent molecules. This is done in section III.B by first presenting three illustrative AIMD simulations of the reaction between Fe^{III} and H_2O_2 in water, which show the spontaneous formation of the iron(III) hydroperoxo species, followed by the characterization of Fe(III)OOH(aq). We have computed the vibrational spectra for the iron(III) hydroperoxo species in both the high-spin ($S = 5/2$) and low-spin ($S = 1/2$) states and have compared these to experimental Raman spectra. For the second step in the Fenton-like mechanism, the O−O homolysis of the iron(III) hydroperoxo species, producing the ferryl ion and a hydroxyl radical is found to be a likely candidate by our static DFT calculations in vacuo. The free energy barrier for this step was computed in aqueous solution using the method of constrained molecular dynamics and thermodynamic integration, the results of which are presented in section III.C. The paper ends with conclusions in section IV.

II. Computational Details

The electronic structure calculations to compute the energies, geometry optimizations, and frequencies of the molecules and hydrated iron complexes in vacuo were performed at the DFT level of theory (see, e.g., ref .34), as implemented in the Amsterdam Density Functional package ADF.[35] We used the Becke-88 gradient-corrected exchange functional[36] and the Perdew-86 gradient-corrected correlation functional.[37] The Kohn−Sham orbitals were expanded in a large even-tempered all-electron Slater-type basis set containing: 4 s, 2 p, and 1 d functions for hydrogen; 6 s, 4 p, 2 d, and 1 f functions for oxygen; and 11 s, 7 p, 5 d, and 1 f functions for iron.[38] The ab initio (DFT) molecular dynamics calculations of the systems including the solvent environment were done with the Car−Parrinello (CP) method[39] as implemented in the CP−PAW code developed by Blöchl.[40] The one-electron valence wave functions were expanded in an augmented plane wave basis up to a kinetic energy cutoff of 30 Ry. The frozen-core approximation was applied for the 1s electrons of O and up to 3p for Fe. For the augmentation for H and O, one projector function per angular-momentum quantum number was used for s- and p-angular momenta. For Fe, one projector function was used for s- and p- and two for d-angular momenta. The characteristic feature of the Car−Parrinello approach is that the electronic wave function, i.e., the coefficients of the plane wave basis set expansion, are dynamically optimized to be consistent with the changing positions of the atomic nuclei. The mass for the wave function coefficient dynamics was $\mu_e = 1000$ au, which limits the MD time step to $\delta t = 0.19$ fs. To maintain a constant temperature of $T = 300$ K, a Nosé thermostat[41] was applied with a period of 100 fs. Periodic boundary conditions were applied to the cubic systems containing one iron ion, one hydrogen peroxide molecule, and 31 water molecules. The size of the cubic box was 9.900 Å. The positive charge of the systems was compensated by a uniformly distributed counter charge.

III. Results

We assume, as is usually done, that the initial step in Fenton and Fenton-like chemistry is the nucleophilic addition of hydrogen peroxide to the iron complex by exchanging with a water ligand in the hydration shell.[42] In the next section (III.A), we discuss the energetics of various reactions starting from the $[Fe^{II}(H_2O)_5(H_2O_2)]^{2+}$ and $[Fe^{III}(H_2O)_5(H_2O_2)]^{3+}$ complexes in order to investigate the thermodynamic possibilities and impossibilities. Figure 1 shows the geometry-optimized structures of these two complexes in vacuo. Later, in section III.B, we will show an illustrative pathway of the reaction of H_2O_2 with Fe^{3+} in water, which includes the coordination process.

TABLE 1: DFT-BP Reaction Energies (kcal/mol) Starting with Either an Aqua Iron(II) Complex ($n = 2$) or an Aqua Iron(III) Complex ($n = 3$) in Vacuo

	gas-phase reaction	Fe(II)	Fe(III)	Fe(III)OH^-
A	$Fe^{n+}(H_2O)_6 \rightarrow Fe^{n+}(H_2O)_5 + H_2O$	22.1	45.7	24.7
B	$Fe^{n+}(H_2O)_5(H_2O_2) \rightarrow Fe^{n+}(H_2O)_5 + H_2O_2$	22.8	46.4	25.4
C	$Fe^{n+}(H_2O)_5(H_2O_2) \rightarrow Fe^{(n+1)+}(H_2O)_5(OH^-) + HO\bullet$	20.7	60.8	38.5
D	$Fe^{n+}(H_2O)_5(H_2O_2) \rightarrow Fe^{(n+2)+}(H_2O)_5(O^{2-}) + H_2O$	-8.0	56.9	9.6
E	$Fe^{3+}(H_2O)_5(H_2O_2) + H_2O \rightarrow Fe^{3+}(H_2O)_5(OOH^-) + H_3O^+$		−156	
F	$Fe^{3+}(H_2O)_5(H_2O_2) + H_2O \rightarrow Fe^{3+}(H_2O)_4(OH^-)(H_2O_2) + H_3O^+$		−145	
G	$Fe^{3+}(H_2O)_5(OOH^-) \rightarrow Fe^{2+}(H_2O)_5 + HOO\bullet$		36.8	40.6
H	$Fe^{3+}(H_2O)_5(OOH^-) \rightarrow Fe^{3+}(H_2O)_5 + HOO^-$		417	281
I	$Fe^{3+}(H_2O)_5(OOH^-) \rightarrow Fe^{4+}(H_2O)_5(O^{2-}) + HO\bullet$		42.6	26.1
J	$Fe^{3+}(H_2O)_5(OOH^-) \rightarrow Fe^{5+}(H_2O)_5(O^{2-}) + HO^-$		444	281

The last column shows the reaction energy starting with iron(III) ($n = 3$) but with one water ligand replaced by a hydroxo ligand, so that the complex has the same total charge as the iron(II) complex. Thus, for the last column, reaction A transforms to $Fe^{3+}(OH^-)(H_2O)_5 \rightarrow Fe^{3+}(OH^-)(H_2O)_4 + H_2O$, and so forth for the other reactions B−J.

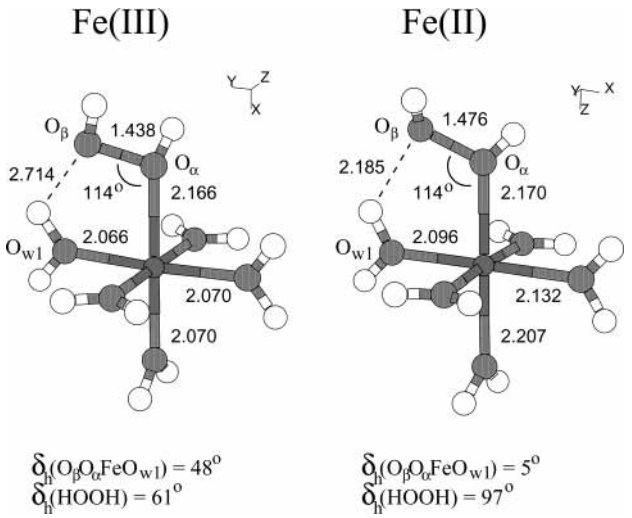

Figure 1. Optimized ground-state structures of $[Fe^{III}(H_2O)_5(H_2O_2)]^{3+}$ (left-hand-side) and $[Fe^{II}(H_2O)_5(H_2O_2)]^{2+}$ (right-hand-side).

A. Elementary Fenton and Fenton-like Reactions in Vacuo. We have computed the reaction energies of the elementary Fenton and Fenton-like reactions of the hydrated iron complexes in vacuo, among which are the ones mentioned in the Introduction (eqs 1−6), and compiled the results in Table 1. The first two columns of numbers on the left-hand side show the reaction energies in kcal/mol with an iron(II) complex and an iron(III) complex as the reactant, respectively. Hydrated metal ions can be acidic, the acidity increasing with increasing oxidation state of the metal ion. For example, the acidity constant of $[Fe^{III}(H_2O)_6]^{3+}$ is $pK_a = 2.2$,[43] so that in aqueous solution hydrolysis easily takes place to form the iron(III) hydroxo complex $[Fe^{III}(H_2O)_5(OH)]^{2+}$ and a free hydronium ion. As we shall see, the lowering of the total charge on the metal complex from 3+ to 2+ has a significant effect on the reactivity. The reaction energies of the present elementary reactions starting from such an iron(III) hydroxo complex are given in the last column of Table 1. Deprotonation of an iron(II) complex is less likely. The acidity constant of hexaaquairon(II) is $pK_a = 9.5$,[44] so that the $[Fe^{II}(H_2O)_5(OH)]^+$ complex forms an improbable starting species.

Starting from hexaaquairon complexes, we see, after comparing reactions A and B, that the ligand exchange of an aqua ligand by hydrogen peroxide is almost thermoneutral but that the water (and H_2O_2) ligands are much more strongly bonded to the 3+ charged iron(III) complexes than to the 2+ charged iron(II) and iron(III) hydroxo complexes (by more than 20 kcal/mol). The production of a free hydroxyl radical, starting from hydrogen peroxide coordinated to iron(II) (as in the Haber and Weiss mechanism, eq 1), costs 20.7 kcal/mol (reaction C in Table 1), a reduction of 39.2 kcal/mol with respect to the dissociation of free hydrogen peroxide into two hydroxyl radicals ($\Delta E = 59.9$ kcal/mol at the same level of theory and 54 kcal/mol including the zero-point energy, in reasonable agreement with the experimental value at 25 °C of 51.2 kcal/mol). Instead, iron(III) does not catalyze the hydrogen peroxide O−O bond dissociation (reaction D, 2nd column), as we see that for pentaaquairon(III) hydrogen peroxide the O−O dissociation and free OH• radical formation is even slightly more endothermic than it is for free hydrogen peroxide (by 1 kcal/mol). The OH• radical produced in reaction C can also abstract the hydrogen from the produced hydroxo ligand to form the ferryl ion ($[Fe^{IV}(H_2O)_5O]^{2+}$) and a water molecule, following the Bray and Gorin mechanism (eq 2) when starting from $[Fe^{II}(H_2O)_5(H_2O_2)]^{2+}$ or the $[Fe^{V}(H_2O)_5O]^{3+}$ species and H_2O when starting from $[Fe^{III}(H_2O)_5(H_2O_2)]^{3+}$ (reaction D in Table 1). In the first case, the overall reaction is exothermic by 8 kcal/mol, but starting with iron(III), the formation of the oxo species is again energetically very unfavorable ($\Delta E = 56.9$ kcal/mol). These numbers clearly show, in the first place, that the highly reactive OH• radical and high-valent iron oxo species are much more easily formed from Fenton's reagent (Fe^{2+}/H_2O_2) than from the Fenton-like reagent (Fe^{3+}/H_2O_2), confirming the experimentally observed difference in oxidative reactivity between the two reagents. In the second place, reactions C and D indicate that the ferryl ion is a much more likely candidate for the active species in Fenton chemistry than the free OH• radical. In refs 5−7 and 45, we discussed the Fenton reagent more extensively and showed that in the two-step process that leads to formation of the ferryl ion, the highest of the two transition states is only 6 kcal/ mol. We also investigated the reactivity of the ferryl ion toward organic substrates by simulating the oxidation of methane to methanol by the ferryl ion.[46] We will now continue to focus solely on the Fenton-like reagent.

The formation of the iron(III) hydroperoxo species from iron(III) hydrogen-peroxide in aqueous solution (eq 3), which is believed to be the initial step in Fenton-like chemistry (reaction E in Table 1), is poorly modeled in vacuo. The absolute reaction energies of such charge-separation reactions are typically highly overestimated, due to the omission of the screening of the solvent and the energies of solvation. The hydrolysis of hexaaquairon(III) for instance, forming pentaaqua hydroxo iron(III) by donating a proton to a water molecule in vacuo, results in an energy gain of 145 kcal/mol, whereas the experimental acidity constant of $pK_a = 2.2$ indicates an (free) energy loss of 3 kcal/mol. However, we can nevertheless compare the reaction energies of charge-separation processes for which the solvent effects are expected to be similar. Hydrolysis of coordinated

TABLE 2: Elongation of the Fe−O Bond Length, rFeO, or the O−O Bond Length, rOO, in the $[Fe^{III}(H_2O)_5(OOH)]^{3+}$ Complex, in Vacuo by a Few Tenths of an Ångström, Shows a Significant Accumulation of Spin Density on the Leaving OH or OOH Fragment, Respectively, Irrespective of the Spin State ($S = 5/2$ or 3/2), Showing that in Both Cases the Fragments Are Radicals and not Ions

	E_0	*r*FeO	*r*OO	*s*Fe	*s*OH	*s*OOH
	spin state $S = 5/2$					
ground-state geometry	0.0	1.898	1.385	4.1	0.2	0.7
elongated *r*FeO	19.7	2.400		3.9		0.9
elongated *r*OO	37.5		2.400	3.2	1.0	
	spin state $S = 3/2$					
ground-state geometry	4.5	1.769	1.415	2.9	-0.1	-0.1
elongated *r*FeO	26.1	2.400		3.8		-1.0
elongated *r*OO	34.8		2.400	3.4	-1.2	

H_2O in pentaaquairon(III) hydrogen peroxide (reaction F in Table 1), for example, is not expected to be much different from the hydrolysis of hexaaquairon(III), and the reaction energies in vacuo are indeed in both cases found to be −145 kcal/mol. Now we can compare reactions E and F, assuming no large differences in energies of solvation for the products, and conclude that the formation of the iron(III) hydroperoxo species in aqueous solution indeed is a likely initial step in Fenton-like chemistry and that the hydrolysis of the H_2O_2 ligand is probably even favored over the hydrolysis of a H_2O ligand. Nevertheless, we want to stress that the proper inclusion of the solvent effects is required to accurately model this first step in Fenton-like chemistry.

Reactions G−J in the table are possible reactions of a second step, in which the iron(III)−hydroperoxo species forms very reactive particles such as radicals and high-valent iron oxo species. Starting with the homolysis of the Fe−O or O−O bond (G and I) in vacuo, we note that the reaction energies of 36.8 and 42.6 kcal/mol are rather endothermic. An important difference between the two reactions is that although they both produce highly reactive radicals, in the Fe−O homolysis (G) the formal oxidation state of iron is lowered, whereas in the O−O homolysis (I) the formal oxidation state of iron increases. As the acidity of hydrated metal ions increases with the oxidation state of the metal (see before), prior hydrolysis of the metal complex works in opposite directions for the two homolysis reactions. Taking the hydrolysis effect into account results in O−O homolysis, forming a probable second step in Fenton-like chemistry, with a reaction energy of 26.1 kcal/mol in vacuo, comparable to the initial ligand expulsion step, reaction A (see the third column of Table 1 for the reaction energies when first hydrolysis of an H_2O ligand has occurred).

Continuing with the heterolysis of Fe−O bond or O−O bond (reactions H and J, respectively), we see that these charge-separation processes result in very high values for the reaction energies in vacuo (as seen before for formation of the iron(III) hydroperoxo species, reaction E, but this time uphill). These calculations are for the isolated products, i.e., they involve full charge separation without screening by the solvent. Even in vacuo the formation of product complexes could be much less unfavorable than full separation of the products. However, if we regard the reactant complexes $[Fe(H_2O)_5O]\cdots OH$ and $[Fe(H_2O)_5]\cdots OOH$ with relatively small elongated bond distances *r*(OO) and *r*(FeO), respectively (instead of infinitely separated products as in Table 1), the production of the radicals (i.e., homolysis) is preferred over that of the anions (i.e., heterolysis). This is shown in Table 2, where we compare the spin densities on the produced OH and OOH fragments for the complexes with a total spin equal to either $S = 5/2$ or 3/2. For large enough separations, the $S = 5/2$ and 3/2 products should converge to the same results in the case of radical formation (whether OH• or OOH•), with only opposite signs for the spin on the leaving fragments in the two different overall spin states. Already for the small elongations shown in the table we see in all four elongated cases a significant accumulation of spin density on the leaving fragments, indicating the formation of radicals rather than incipient formation of partially charged OH^- or OOH^- species.

However, in aqueous solution, the differences in reaction energies between the heterolysis reactions, H and J, and the homolysis reactions, G and I, are expected to be much smaller, due to the much larger hydration energies of the ions compared to that of the radicals. The enthalpy of hydration for the OH^- ion is known to be −87 kcal/mol, and the increase of the positive charge on the iron complex left behind from 2+ to 3+ may lead to a similar additional stabilization from stronger solvation. Clearly, we would have to include the full solvent effects to realistically compare the energetics of reactions G−J. In the present work, we will start with the inclusion of solvent effects by computing the free energy barrier for the O−O homolysis reaction in aqueous solution (section III.C). This reaction (I) appears to be the most likely one on energetic grounds and is particularly interesting because both products, the OH• radical and the ferryl ion, are very reactive and are expected to be active intermediates in Fenton oxidation reactions. The other possible reactions are left for future work, but it should also be noted that further technical development is required to make the study of those reactions with AIMD simulations possible. The O−O heterolysis (J) requires a spin flip as the ground-state state of the reactants has $S = 5/2$, whereas the iron(V)oxo product has $S = 3/2$. This jump from one spin surface to another during a Car−Parrinello molecular dynamics simulation of the reaction in aqueous solution is presently not yet possible. The CPMD simulation of the Fe−O dissociation reactions requires the as yet impossible constraining of the relevant electron onto either the OOH fragment or the iron complex.

Summarizing, the static DFT calculations show that for iron-(III) hydrogen-peroxide the direct formation of the OH• radical (C) or the high-valent iron oxo species(D) is energetically much less favorable than for iron(II) hydrogen-peroxide. Second, the acidity of iron(III) complexes is expected to play an important role as the hydrolysis of a water ligand lowers the reaction energies dramatically, particularly in the case of the iron(V)-oxo complex formation (D). In the third place, hydrolysis of the H_2O_2 ligand of $[Fe^{III}(H_2O)_5(H_2O_2)]^{3+}$, producing the iron-(III) hydroperoxo species (E) is energetically favored over hydrolysis of a water ligand (F). In the next section, we will show that in aqueous solution indeed the hydrolysis of the H_2O_2 ligand (E) forms the initial step in the Fenton-like chemistry, so that for the next step the transformation of the iron(III) hydroperoxo species becomes important. In the fourthplace, possible second-step transformations are the homolysis and heterolysis of the Fe−O bond and the O−O bond, of which the homolysis reactions are favored in vacuo, but no fair comparison can be made for the solvated case without the proper inclusion of the solvent effects. However, homolysis of the O−O bond is already seen to become particularly interesting when a second hydrolysis (of a water ligand) takes place. We will investigate the O−O bond homolysis and the simultaneous second hydrolysis in aqueous solution in section III.C.

B. First Reaction Step in Fenton-like Chemistry in Water: Formation and Characterization of the Iron(III) Hydroperoxo Species. *(a) Formation.* In this section we will

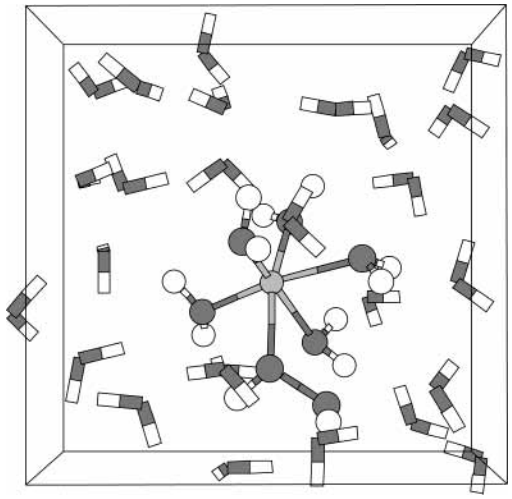

Figure 2. Initial configuration of H_2O_2 coordinated to Fe^{3+} surrounded by 31 water molecules in a cubic box with periodic boundary conditions. The pentaaqua iron(III) hydrogen peroxide complex is shown in ball−stick representation, while, for clarity, the solvent molecules are depicted by sticks.

describe the results of our study of the most likely intermediate formed in a mixture of iron(III) ions and hydrogen peroxide in water. We will follow the same approach as in our previous work[7] on the active intermediate formed from iron(II) and hydrogen peroxide, which makes it easy to compare the reactions with each other. In this previous work on Fenton's reagent, we showed two illustrative pathways of the reaction between Fe^{2+} and H_2O_2 in water producing the high-valent iron−oxo species $[Fe^{IV}O]^{2+}$. The ferryl ion formation occurred either in two steps, via an iron(IV) dihydroxo intermediate ($[Fe^{IV}(OH)_2]^{2+}$), if we started from a $[Fe^{II}(H_2O_2)]^{2+}$ complex, or via a more direct "rebound" mechanism if we started from separated Fe^{2+} and H_2O_2, thus including the coordination process of H_2O_2 to an empty iron(II) site. The $[Fe^{II}(H_2O_2)]^{2+}$ complex was not found to be a stable intermediate in aqueous solution, unlike $[(H_2O)_5Fe^{II}(H_2O_2)]^{2+}$ in vacuo.

For the present reaction of hydrogen peroxide with iron(III), we performed a Car−Parrinello MD simulation of H_2O_2 coordinated to Fe^{3+}, surrounded by 31 water molecules in a cubic box with periodic boundary conditions. Figure 2 shows the initial configuration, which we obtained from the study of the $[Fe^{II}(H_2O_2)]^{2+}$ complex in water and by removing in that configuration one spin-down electron from the system. The total spin was thus $S = 5/2$, and the total charge equaled 3+, which was counterbalanced by a uniformly distributed 3− charge. We relaxed the system to the new situation, by an MD run of 3.5 ps. During this time of equilibration, bond constraints were applied to the Fe−O and O−O bonds, fixing these bond lengths to their equilibrium distances to prevent a premature breakup of the complex by the unrelaxed environment. Next, we removed the constraints and followed the evolution of the $[Fe^{III}(H_2O_2)]^{3+}$ complex in water for 5 ps.

Already in the equilibration phase, hydrolysis had taken place on the α-oxygen of the ligated hydrogen peroxide (α denotes the oxygen connected to iron), donating the proton to the water solvent

$$[(H_2O)_5Fe^{III}(H_2O_2)]^{3+} + H_2O \rightarrow [(H_2O)_5Fe^{III}(OOH)]^{2+} + H_3O^+ \quad (7)$$

Our simulation thus started with an iron(III) hydroperoxo complex and a hydronium ion in water, and no further spontaneous transformation took place during the 5 ps of molecular dynamics. The oxygen−oxygen bond did not break but instead fluctuated around an average bond length of $R_{OO} = 1.466$ Å, contrary to the oxygen−oxygen bond of hydrogen peroxide coordinated to iron(II) which was found to cleave spontaneously in aqueous solution. Also, the aqueous proton was not observed to jump back on the hydroperoxo ligand during our simulation, as with the dynamic equilibria we have, for instance, seen for hydrolysis of aqua ligands of hexaaquairon(III) (see before) and the $[(H_2O)_4Fe^{IV}(OH)_2]^{2+}$ complex.[6] The OH bond length fluctuations of the aqua ligands were significantly larger than the ones in hexaaquairon(II), with maxima of $R_{OH}^{max} = 1.4$ Å ($R_{OH}^{max} = 1.1$ Å in hexaaquairon(II)), almost donating a proton to the solvent but never dissociating completely. This indicates that the acidity of $[(H_2O)_5Fe^{III}(OOH)]^{2+}$ is between that of hexaaquairon(II) and hexaaquairon(III).

To make sure that the hydroperoxo ligand formation (during the equilibration phase) was not the result of nonequilibrium solvent effects, we started a second MD simulation from a configuration of the equilibration phase at a time just before the hydrogen peroxide hydrolysis took place. This time we constrained the $O^{\alpha}-H$ bond length to prevent hydrolysis during a 1.2 ps equilibration run, after which we removed the constraint and again followed the evolution of the system. Although during most of the equilibration time an aqua ligand donated a proton to the solvent (eq 8)

$$[(H_2O)_5Fe^{III}(H_2O_2)]^{3+} + H_2O \leftrightarrow [(H_2O)_4Fe^{III}(OH)(H_2O_2)]^{2+} + H_3O^+ \quad (8)$$

this proton is united with the hydroxo ligand again at the end of the equilibration, so that indeed we started with a $[(H_2O)_5Fe^{III}(H_2O_2)]^{3+}$ complex in water. After 0.2 ps, hydrolysis of the coordinated hydrogen peroxide takes place so that the $Fe^{III}OOH$ moiety is formed, which again remains stable for the next 1.75 ps, after which we stopped the computation. Clearly, this second simulation shows that the H_2O_2 ligand hydrolysis was not an effect of the unrelaxed environment (which was not clear from the first simulation). Second, the higher stability of the O−O bond compared to the iron(II) hydrogen peroxide case is not a result of the H_2O_2 hydrolysis, since no O−O lysis occurred spontaneously when only the O^{α}-H bond length was constrained.

Finally, we performed a last AIMD simulation in which we also wanted to include the formation of a coordination bond of hydrogen peroxide to a vacant coordination site of iron(III). Starting with a random configuration in which the solvated reactants are separated from each other a certain distance is however very unpractical, because the probability of a spontaneous coordination is too small to make an observation likely in the relatively short time of a typical AIMD simulation. We therefore applied a simple device, which had worked very well for the iron(II)/H_2O_2 system already.[7] We carried out a constrained AIMD simulation of hydrogen peroxide coordinated to iron(III) in water. The O−O bond, the $Fe-O^{\alpha}$ bond, and the O^{α}-H bond were fixed to their equilibrium distances, and also a bond constraint was applied to the distance between the peroxide's O^{β} and the hydrogen of an adjacent water ligand, fixing this distance to $R_{OH} = 2.0$ Å. The small strain induced in the five-membered ring which is closed by the R_{OH} constraint (see also Figure 1) was enough to pull hydrogen peroxide from the aquairon complex when we released all constraints, except the $O^{\alpha}-H$ bond constraint. This process is illustrated in Figure 3, showing the distances $Fe-O^{\alpha}$, $Fe-O^{\beta}$, $O^{\alpha}-O^{\beta}$, and $O^{\alpha}-H$ as a function of time, starting just before the moment we released these bond constraints.

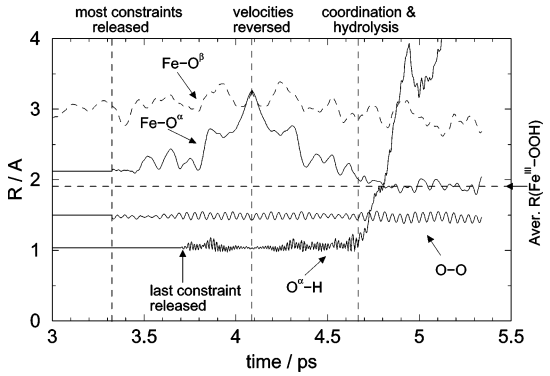

Figure 3. The Fe−O$^{\alpha}$, Fe−O$^{\beta}$, O$^{\alpha}$−O$^{\beta}$, and O$^{\alpha}$−H distances as a function of time during the AIMD simulation of H_2O_2 and Fe^{3+} in water, starting from the last part of the equilibration phase (coordinated Fe−H_2O_2 complex). After $t = 3.32$ ps, Fe−O$^{\alpha}$ increases as H_2O_2 leaves the coordination shell. At a separation of more than 3 Å, all velocities are reversed and simulation shows the process of coordination of hydrogen peroxide occurring almost simultaneous with the hydrolysis, forming the iron(III) hydroperoxo moiety.

After release of all constraints except the O$^{\alpha}$−H bond constraint, at $t = 3.32$ ps, the Fe−O$^{\alpha}$ bond starts to break, which is visible in Figure 3 as the appearance of oscillations with increasing amplitude of $R_{Fe-O^{\alpha}}$, and at $t > 3.9$ ps, Fe and O$^{\alpha}$ clearly separate. During the dissociation process, at $t = 3.72$ ps, we also released the O$^{\alpha}$−H bond constraint. At time $t >$ 4.1 ps, we now have a situation where the Fe−O$^{\alpha}$ distance has increased to more than 3 Å, i.e., the iron aqua complex and H_2O_2 are separated from each other by at least 3 Å, with velocities that will lead to further separation. At this point, we reverse all the velocities (including those of the electronic wave function degrees of freedom and the Nosé thermostat variable) so that the reactants will now approach each other in the same way as they separated. The difference of course is that the O$^{\alpha}$−H is now free to dissociate. In Figure 3, we indeed see that as soon as hydrogen peroxide coordinates to the Fe^{3+} ion, the O$^{\alpha}$−H bond breaks, the proton moves into the solvent, and the iron(III) hydroperoxo complex is being formed.

These illustrative pathways confirm our inference from the calculation in a vacuum (Table 1) that formation of the Fe(III)-(OOH) species is a likely candidate for the initial step in the Fenton-like reaction and, second, that the oxygen−oxygen bond does not break so easily as in hydrogen peroxide coordinated to iron(II), which ultimately led to the ferryl ion as the most likely active intermediate in the Fe(II) catalysis. Moreover, formation of $[Fe^{III}(H_2O)_5(OOH)]^{2+}$ seems much more likely than formation of $[Fe^{III}(H_2O)_4(OH)(H_2O_2)]^{2+}$, in agreement with Table 1. This implies that as the second step of the Fenton-like reaction we should investigate the subsequent transformation of Fe(III)(OOH). This will be done in section III.C. However, we will first investigate further the iron(III) hydroperoxo complex itself, making a connection with the experimental characterization of this moiety by vibrational spectroscopy of this metal−ligand system in various solvents and with different ligand environments.

(b) Characterization: Fe(III)−OOH Vibrations. Spectroscopic experiments have indicated that the spin state of Fe(III)-OOH complexes has a strong effect on the Fe−O and O−O bond strengths.[47,48] Resonance Raman spectroscopy on low-spin iron(III) hydroperoxo complexes with large ligands such as N4Py (*N*,*N*-bis-(2-pyridylmethyl)-*N*-bis(2-pyridyl)methylamine),[49] TPA (tris-(2-pyridylmethyl)-amine),[48] and TPEN (*N*,*N*,*N*′,*N*′-tetrakis-(2-pyridylmethyl)ethane-1,2-diamine)[50] show O−O vibrations with frequencies between 789 and 801 cm^{-1}

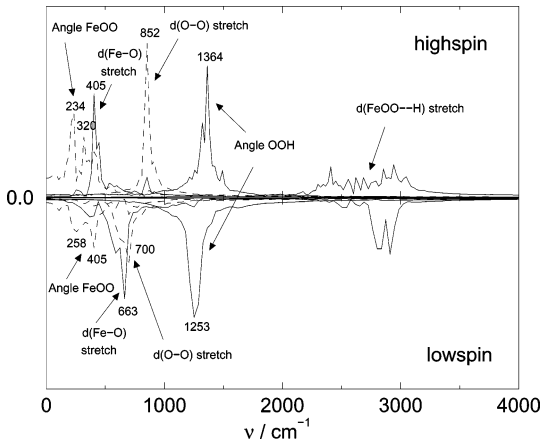

Figure 4. Frequency spectra of the $Fe^{III}OOH$ species in water in the electronic high-spin state $S = 5/2$ (upper half) and in the low-spin state $S = 1/2$ (lower half).

and Fe−O vibrations between 617 and 632 cm^{-1}. High-spin complexes show stronger O−O bonds ($\nu_{O-O} > 844$ cm^{-1}) and weaker Fe−O bonds ($\nu_{Fe-O} < 503$ cm^{-1}). The spin state is normally dictated by the ligand field splitting 10*Dq* caused by the ligands, but in our computer experiments we can simply fix the number of spin-up and spin-down electrons. We have thus calculated the Fe(III)OOH frequencies of the complex in water at $T = 300$ K for both spin states. This was done by performing an AIMD simulation for each spin state starting from the last frame of the first simulation of Fe(III)OOH (see previous section). The hydronium ion in the solvent was replaced with a water molecule to avoid the influence it could have on the vibrations of the complex. We calculated a 2.5 ps AIMD trajectory, from which the last 1.5 ps was used to calculate the velocity autocorrelation of specific vibrations, such as the oxygen−oxygen bond stretching $d_{OO}(t)$. The Fourier transformation of these velocity autocorrelation functions gives the vibration spectra shown in Figure 4. The peaks shown in Figure 4 are rather broad, which is partly due to the relatively short simulation time (limited statistics). Nevertheless, the statistics are sufficient to clearly resolve the large differences between the low-spin and high-spin spectra.

The OH stretch vibration in the hydroperoxo ligand gives rise to a broad region of peaks around 2500−3000 cm^{-1} in the $S = 5/2$ state, whereas these peaks are more localized in the low-spin state. In the simulation (and also in experiments[51]), the OH stretch frequency decreases when the hydrogen forms a hydrogen bond with a solvent water molecule. The shorter (stronger) the hydrogen bond, the lower the OH frequency. The average hydrogen bond length between the hydroperoxo hydrogen and the nearest solvent oxygen is 0.08 Å shorter in the high-spin state than in the low-spin state, while the average OH bond length in the hydroperoxo ligand is 0.01 Å longer. This could be an indication that the hydroperoxo ligand is more easily deprotonated in high-spin complexes, giving rise to the peroxo ligand, than in low-spin complexes.

The O−O stretch vibration decreases from 852 to 700 cm^{-1} when going from the high-spin state to the low-spin state and the Fe−O stretch vibration increases from 405 to 663 cm^{-1}, in agreement with the trend found with Raman spectroscopy for different complexes. For comparison, we also optimized the geometry for the $[Fe^{III}(H_2O)_5(OOH)]^{2+}$ complex in vacuo for the $S = 1/2$ and 5/2 states and calculated the vibrational frequencies in the harmonic approximation. The results are shown in Table 3 together with a compilation of values for the O−O and Fe−O stretch vibrations obtained using Raman

TABLE 3: Fe(III)OOH Vibrations Calculated for the Hydrated Complex in Vacuo and in Aqueous Solution Compared to Experimental Raman Frequencies of Low-Spin and High-Spin Complexes

	∠FeOO	*d*FeO	*d*OO	∠OOH	*d*OH
		low-spin calculations			
$(H_2O)_5Fe^{III}OOH$ (g)[a]	253, 326	626	810	1291	3544
$(H_2O)_5Fe^{III}OOH$ (aq)[b]	258, 405	663	700	1253	2500-3000
		experiment			
$[(N_4Py)Fe(OOH)]^{2+}$ [c]		632	790		
$[(TPA)Fe(OOH)]^{2+}$ [c]		626	789		
$[(TPEN)Fe(OOH)]^{2+}$ [d]		617	796		
$[(trispicen)Fe(OOH)]^{2+}$ [d]		625	801		
$[(trispicMeen)Fe(OOH)]^{2+}$ [d]		617	796		
		high-sp in calculat ions			
$(H_2O)_5Fe^{III}OOH$ (g)[a]	180, 209	445	980	1366	3514
$(H_2O)_5Fe^{III}OOH$ (aq)[b]	234, 320	405	852	1364	2000−3000
		experiment			
$[(TPEN)Fe(-\eta^2\text{-}OO)]^{2+}$ [d]		468	821		
$[(trispicMeen)Fe(-\eta^2\text{-}OO)]^{2+}$ [d]		468	820		
$[Fe(EDTA)(-\eta^2\text{-}OO)]^{3-}$ [e]		459	816		
$[Fe(EDTA)(-\eta^2\text{-}OO)]^{3-}$ [f]		472	824		
oxyhemerythrin$(-\eta^1\text{-}OOH)$[g]		503	844		

spectroscopy on several low-spin and high-spin complexes. The O−O stretch vibration is significantly lower in the solvent than in the gas-phase complex. This decrease, indicating a weakening of the O−O bond in aqueous solution, is due to the interaction of solvent water molecules with the hydroperoxo group. Not only the hydrogen but also both oxygens are involved in hydrogen bonds with the solvent. Integration of the radial distribution functions (data not shown) obtained from the first 5 ps simulation of high-spin Fe(III)OOH in water (see previous paragraph) gives an average of 1.6 solvent hydrogens within a 2.3 Å radius of O^{β} and 0.8 (other) solvent hydrogens within a 2.3 Å radius of O^{α}. Surprisingly, the static DFT results in vacuo for the low-spin O−O and Fe−O vibrations compare better with the experimental results than the ones obtained from the dynamics in aqueous solution at $T = 300$ K. This could be due to (again) the aqueous solvent interactions with the hydroperoxo ligand in the simulation, whereas the Raman spectroscopy studies using the hydrophobic pyridine-based ligands as N4Py, TPA, TPEN, trispicen, and trispicMeen typically took place in solvents such as acetone and acetonitrile. Another factor is, of course, the ligand field on the aqua ligated iron in the simulation, which is quite different from the ligand fields on iron complexed by these large nitrogen multidentate ligands used in the experiments. Comparison of our high-spin results with the only η^1-OOH complex listed, namely, oxyhemerythrin in aqueous solution, indicates that both factors could play a role: the Raman O−O stretch vibration now agrees much better with the AIMD result as in both results the solvent used is water, which interacts with the hydroperoxo ligand, and second, the Fe−O stretch vibrations are still a bit off due to the different ligand field (note that oxyhemerythrin is a diiron species: L−Fe(III)−O−Fe(III)−OOH).

In conclusion, we find that indeed the spin state is an important factor for the O−O and Fe−O bond strengths in Fe(III)OOH complexes. The ligands (chelating agents) used in Fenton-like chemistry are therefore expected to directly influence the chemistry, because ligands inducing a large ligand field give rise to low-spin Fe(III)OOH complexes with stronger Fe−O bonds and weaker O−O bonds compared to the Fe−O and O−O bonds in the high-spin complexes which occur with ligands inducing a small ligand field. For the suggested second-step reactions following the initial Fe(III)OOH formation (eqs 4−6), the low-spin complexes thus promote the steps involving O−O lysis but make the steps involving Fe−O bond breaking even more unfavorable.

C. Second Step in Fenton-like Chemistry in Water: Calculation of the Free Energy Barrier of O−O Homolysis of Fe(III)OOH. One of the proposals for the second reaction step in the oxidation catalysis by the Fenton-like reagent involves homolysis of the oxygen−oxygen bond of the iron(III) hydroperoxo species, producing an OH• radical and the ferryl ion (eq 5). We studied this reaction in detail, since it has emerged from our static DFT calculations as a likely second reaction step, in particular when the hydrolysis of a water ligand is simultaneously taken into account.

We performed constrained AIMD simulations to calculate the free energy profile for the oxygen−oxygen bond homolysis reaction of the $[Fe^{III}(H_2O)_5OOH]^{2+}$ complex into an iron(IV)-oxo species and an OH• radical in water (see for the method of constrained molecular dynamics refs 52−55). The oxygen−oxygen bond length R_{OO} was taken as the constrained reaction coordinate, which seems intuitively a good choice that includes the most important contribution to the intrinsic reaction coordinate. Nevertheless, this choice has two drawbacks that we want to mention. First, this simple constraint does not include environmental degrees of freedom (e.g., via coordination constraints), which we previously showed to be very important when the reaction involves ions (i.e., when large changes in the charge on fragments induces large, but slow, changes in the solvation shells),[13] but is expected to be of minor importance in present case where we deal with a neutral, OH• radical, leaving group. Second, our constraint does not prevent the unwanted side reaction of abstraction of solvent molecule hydrogens by the produced OH• radical. That is, for large values of the constrained reaction coordinate R_{OO}, the OH• radical can abstract a solvent hydrogen forming H_2O while an OH• species "jumps" through the solvent by a chain reaction. The sampled force of constraint will then be, of course, meaningless as it is associated with the force necessary to keep a H_2O molecule (instead of the OH•) constrained to the oxygen of the iron complex. We will therefore take the same approach as was done in the work by Trout and Parrinello, who studied the dissociation of H_2O in water in H^+ and OH^- with the same technique[56] and only calculated the profile up to (or at least very close to) the transition state. Since the subsequent reaction of the OH• "jumping" into the solvent is thermoneutral, the free energy profile of the homolysis is not expected to decrease by more than a few kcal/mol beyond the transition state (due to the increasing entropy of the leaving OH• radical and the solvation of the oxo site). Moreover, the transition-state energy is the more

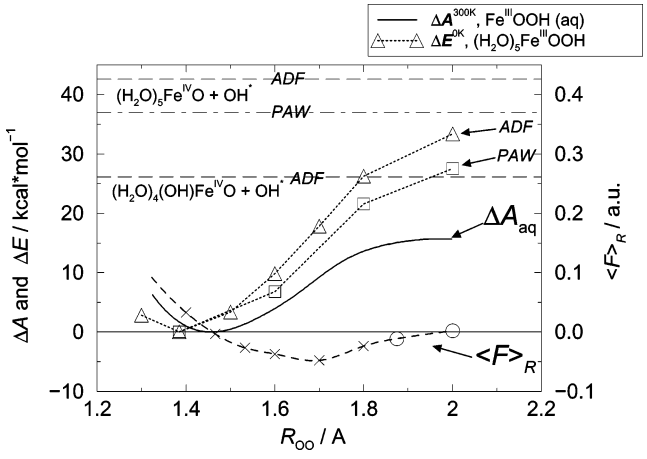

Figure 5. Mean force of constraint $\langle F \rangle_R$ (dashed line; right-hand-side axis) and the Helmholtz free energy ΔA (solid line; left-hand-side axis) versus the oxygen−oxygen distance R_{OO}. The crosses denote the values from constrained MD runs sampled during 2 ps, and the circles denote the average constraint force during 1.3 ps, up to the moment that the OH• radical abstracts a hydrogen from a nearby solvent molecule. The dotted lines give the energies of the hydrated complex in vacuo, calculated with the ADF program (triangles) and with the PAW program (squares). The limits of infinitely far separated products (reaction I in Table 1) are indicated by vertical dashed lines.

important parameter to determine whether the oxygen−oxygen homolysis is indeed a probable mechanism.

Eight constrained AIMD runs were performed with constrained oxygen−oxygen bond lengths varying from R_{OO} = 1.4−2.0 Å. The initial configuration of each constrained simulation was taken from the last frame of the first simulation of hydroperoxo iron(III) in water, including the hydronium ion (see section III.B). For each system, a short AIMD simulation was started to bring R_{OO} to the desired value in 2000 steps. Then equilibration of each system took place for 2 ps, after which the force of constraint was accumulated for another 2 ps. The obtained values for the mean force of constraint are denoted by crosses and circles in Figure 5 and fitted with a quadratic spline. Integration of the mean force of constraint gives the Helmholtz free energy profile $\Delta A(R_{OO})$, where we take the minimum at R = 1.46 Å for the offset of the energy scale (solid line). The circles indicate those constrained simulations during which the $O^{\beta}H$• radical abstracts a hydrogen and transforms into a water molecule. Indeed, this occurs for the R_{OO} values close to the transition state, for which the $O^{\beta}H$ part has acquired enough radical character to abstract a hydrogen when a nearby solvent molecule moves into a suitable position. In both cases (at R_{OO} = 1.875 Å and R_{OO} = 2.000 Å), the hydrogen abstraction occurs after about 1.3 ps simulation. The values for the mean force of constraint denoted by the circles are the averages over these 1.3 ps. After the H abstraction by $O^{\beta}H$•, the force of constraint goes to zero or becomes even slightly positive (repulsive) because the produced water molecule is repelled by the oxo ligand at the short constrained oxygen−oxygen distance rather than attracted like the OH• radical shortly before. For the O−O distance of R_{OO} = 2.000 Å, the average force of constraint (over the 1.3 ps before the H abstraction) is almost equal to zero, which indicates that this O−O distance is indeed very close to the transition state.

The free energy reaction barrier for the homolysis reaction in water is found to be $\Delta A^{\ddagger}$ = 15.7 kcal/mol, which is low compared to the ΔE = 42.6 kcal/mol (ground-state) energy change found for the reaction in vacuo or even the ΔE = 26.1 kcal/mol for the hydrolyzed complexes in vacuo (reaction I in Table 1). We also plotted the contour for the reaction energy ΔE^{0K} of the homolysis of the $[Fe^{III}(H_2O)_5OOH]^{2+}$ complex in vacuo twice (triangles connected by a dotted line and the value for infinite product separation indicated by the vertical dashed line); once computed with the ADF program and once computed with the PAW program. Unfortunately, we find an increasing underestimation of the energy profile with increasing R_{OO}, calculated with PAW compared to the highly accurate (all-electron, large basis set) ADF results, with a maximum difference of 5.6 kcal/mol at R_{OO} = 2.0 Å and at infinite separation. The error does not seem to be due to the plane-wave cutoff of 30 Ry (it is only reduced by 0.5 kcal/mol when going to 50 Ry) and can be attributed to the partial waves for the inner region of the valence electrons and the projector functions for the iron atom used in the PAW calculations. Although bond energies in iron(III) and iron(IV) complexes computed with PAW agree within 2 kcal/mol with those using ADF, we found after extensive tests that the stability of the (formally) Fe^{4+} configuration is overestimated by 5−6 kcal/mol with respect to the (formally) Fe^{3+} configuration. This indicates that the free energy barrier of the homolysis in aqueous solution also has to be corrected for this error so that the true value becomes $\Delta A^{\ddagger} \approx 21$ kcal/mol. Solvent effects thus strongly reduce the transition-state barrier for the O−O homolysis reaction in water. The main contribution to this effect is expected to originate from the larger absolute energy of solvation for the separating transition-state complex (Fe^{IV}=O···OH•) in comparison with the reactant molecule, Fe^{III}OOH. (Note that often reaction barriers are increased in aqueous solution, because the sum of the absolute energies of solvation for two reacting molecules is typically larger than that for the single transition state complex.)

The upper graph in Figure 6 illustrates the transformation of the Fe^{III}−OOH^{-} bond into an Fe^{IV}=O^{2-} bond by showing the average Fe−O^{α} distance as a function of the reaction coordinate. The two dashed lines indicate the average R_{FeO} for the pentaaquairon(III) hydroperoxo complex in water (obtained from the first 5 ps simulation described in section III.B), equal to 1.922 Å and the average R_{FeO} for the ferryl ion in water equal to 1.680 Å. This latter number was obtained from the $[Fe^{IV}O(OH)]^{+}$ moiety produced in the reaction between Fe^{II} and H_2O_2 in water (cf. ref 7), in which indeed a water ligand hydrolyzed to form the OH^{-} ligand, as suggested in section III.A. This apparent increased acidity of the iron(IV) species compared to that of iron(III) is discussed below. Proceeding with the Fe−O distance, we see that R_{FeO} decreases rapidly when the oxygen−oxygen separation becomes larger than 1.7 Å, which indicates the changing character of the metal and the bonds. At the reaction coordinate value of R_{OO} = 2.0 Å, the average R_{FeO} (over the 1.3 ps simulation before the $O^{\beta}H$• radical abstracts a solvent hydrogen) has decreased practically to the average value of free $[Fe^{IV}O(OH)]^{+}$, which indicates that at R_{OO} = 2.0 Å the reaction is close to completion. The open circles in Figure 6 denote the averages over the simulation part after the $O^{\beta}H$• radical transformed into H_2O^{β} by H-abstraction from an adjacent solvent molecule. At R_{OO} = 1.6 Å, the average R_{FeO} is a little larger than expected from the trend. This is the result of proton donation from the iron complex (i.e., hydrolysis) to the aqueous solvent during the constrained simulation at this reaction coordinate value, which we will explain below.

As mentioned before, we expect hydrolysis of water ligands to lower the reaction energy of the oxygen−oxygen homolysis (see the change from 42.6 to 26.1 kcal/mol for reaction I in Table 1), and second, we expect hydrolysis to become more frequent for iron(IV) (product) compared to iron(III) (reactant).

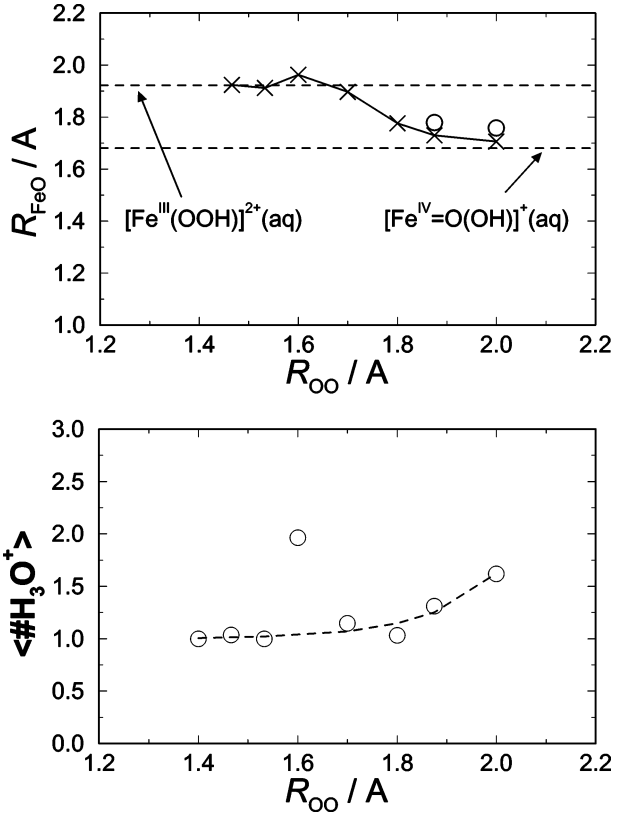

Figure 6. (top) Average Fe−Oα bond length as a function of the constrained reaction coordinate R_{OO}. Two dashed lines indicate the average values for reactant and product iron complexes in solution, respectively. Open circles denote the average R_{FeO} after the product $O^{\beta}H\bullet$ transformed into H_2O by H-abstraction from an adjacent solvent molecule. (bottom) Average number of hydronium ions as a function of the reaction coordinate.

In our short constrained dynamics simulations of the enforced $O^{\alpha}-O^{\beta}$ homolysis in aqueous solution, we can indeed observe these trends by plotting the average number of hydronium ions in the solvent versus the reaction coordinate R_{OO} (see circles in the lower graph in Figure 6 and the dotted lines to guide the eye). The water ligand O−H distances R_{OH} were taken as the order parameters: all 10 $R_{OH} < 1.3$ Å means that no hydrolysis has taken place. At the reactant side (small R_{OO}), hydrolysis is rarely observed during the 2 ps simulations and only the one hydronium ion which we started with (originating from the hydrogen peroxide when it reacted with iron(III), see previous sections) brings the average number to 1 H_3O^+. Going toward higher R_{OO} values, the oxidation state of the iron ion goes to 4+ and the complex is seen to become more acidic, confirming the second trend mentioned. At $R_{OO} = 2$ Å, 62% of the time a (second) proton was donated to the solvent by the complex (in the 1.3 ps before H abstraction by the leaving $O^{\beta}H\bullet$ from a solvent water), which justifies the previous comparison of R_{FeO} with that of the hydrolyzed ferryl ion ($[Fe^{IV}O(OH)]^+$) in the upper graph. At $R_{OO} = 1.6$ Å, the average number of 1.96 hydronium ions seems out of order in this trend. In the simulations, we see that for this run the two hydronium ions are most of the time jumping freely around in the solvent. In the other runs, however, we find that most of the time one of the protons jumps back and forth between the ligand and a solvent water molecule and thus remains in the neighborhood of the complex. Apparently we can separate the ligand hydrolysis into two stages which show resemblance with the dynamics of free hydronium ion transfer in water (cf. ref. 57), namely, (1) a fast process which involves the sharing of the proton by a ligand and a solvent molecule (or two solvent waters for the free hydronium ion, with a frequency $\nu \approx 5$ ps^{-1}) and (2) a much slower process, which is connected to the actual stepwise diffusion of the hydronium ion through the solvent. The latter process concerns changes in the second coordination shell hydrogen bond network, which in water was found to have a frequency of about 0.5 ps^{-1}.[57] Obviously, our 2 ps AIMD simulations are too short to capture good statistics of the slow process, so that in each simulation we either see the excess proton being shared by two water molecules in the solvent (namely, in the run with $R_{OO} = 1.6$ Å) or it is being shared by a ligand and a solvent molecule (as in all other runs). Fortunately, from the distribution in the fast jumping process we have already obtained information on the acidity (i.e., the ability to donate a proton to the aqueous environment) of the iron complex, as shown in Figure 6, but for comparison with experimental pK_a values we need to include also the slower hydronium ion transport. The run with $R_{OO} = 1.6$ Å confirms the first trend mentioned in this paragraph: replacement of a water ligand by a hydroxo ligand facilitates the oxygen−oxygen homolysis. In our constrained MD exercise this is seen by the lower absolute constraint force resulting in a dent in the mean constraint force profile in Figure 5 and also in the R_{FeO} profile in Figure 6. If we could afford better statistics by performing much longer simulations, in principle the two states (pentaaqua versus hydrolyzed tetraaqua hydroxo complex) would be sampled with correct weights, giving the correct mean force of constraint and free energy profile. In our result however, we find for all runs except the one with $R_{OO} = 1.6$ Å mostly the pentaaqua complex, so that we should take into account an overestimation of a few kcal/mol for the free energy barrier. Moreover, if we would be interested in calculating the reaction rate of the O−O homolysis reaction in water we should either control the hydrolysis process by including it in the reaction coordinate or expect a large deviation from the transition-state theory reaction rate and therefore perform the cumbersome computation of the transmission coefficient in the preexponential factor. We can nevertheless conclude that our estimation of the free energy barrier of the O−O homolysis of the iron(III) hydroperoxo intermediate in aqueous solution indicates that this formation of a ferryl ion and the OH• radical is a likely second step in Fenton-like chemistry. Second, the simulations confirm the hypothesis that water ligand hydrolysis plays an important role in the process.

IV. Conclusions

We performed static DFT calculations on the hydrated Fenton-like reagent in vacuo, $[Fe^{III}(H_2O)_5(H_2O_2)]^{3+}$, and ab initio (DFT) molecular dynamics (AIMD) simulations of the Fenton-like reagent in aqueous solution, Fe^{3+}/H_2O_2(aq), to determine and characterize the active intermediates. The static DFT calculations on the hydrated iron(III) complexes in vacuo showed that the direct formation of active intermediates, such as the OH• radical or a high-valent iron oxo species ($[Fe^{V}O]^{3+}$), are endothermic by as much as 61 and 57 kcal/mol, respectively. This is in agreement with the experimentally observed much lower reactivity of the Fenton-like reagent compared to Fenton's reagent (Fe^{II}/H_2O_2), for which we found that the formation of the highly reactive ferryl ion ($[Fe^{IV}O]^{2+}$) is exothermic by 8 kcal/mol in vacuo.

Moreover, our AIMD simulations of the Fenton-like reagent in aqueous solution show that the first reaction step consists of the donation of the α-proton of hydrogen peroxide to the solvent shortly after the hydrogen peroxide coordinates to iron(III), as

also suggested by the static DFT calculations of the aqua-ligated complex in vacuo. The produced $Fe^{III}OOH$ intermediate has previously been proposed to react in a second step via heterolytic or homolytic dissociation of the O−O bond or the Fe−O bond. The very high endothermicy of the two heterolytic (charge separation) reactions, found with static DFT calculations of the aqua-ligated complexes in vacuo, shows the importance of solvent effects. In aqueous solution, these reactions are expected to be much less endothermic due to the high hydration energies of the ionic products. Unfortunatly, it is technically not yet possible to simulate these reactions using AIMD. Also, for the two homolytic dissociations, producing the OH• or OOH• radical, respectively, the solvent effects are shown to be important. Inclusion of the aqueous solution opens the possibility of hydrolysis of aqua ligands of the acidic iron complexes, which we show to have a strong effect on the energetics of the dissociation reactions. Taking such proton donation into account, the static DFT calculations suggest the O−O bond homolysis, producing the ferryl ion and a hydroxyl radical, as a possible second reaction step in the Fenton-like reaction, as the endothermicy of O−O bond homolysis in vacuo is reduced from 43 to 26.1 kcal/mol upon hydrolysis of a water ligand. The AIMD simulations indicate that the solvent effects lower the barrier for O−O bond homolysis in $[(H_2O)_5Fe^{III}(OOH)]^{2+}$ significantly to a free energy barrier at $T = 300$ K in aqueous solution of approximately $\Delta A^{\ddagger} = 21$ kcal/mol with concomitant hydrolysis of a water ligand.

The important iron(III) hydroperoxo(aq) intermediate has been investigated by comparing calculated vibrational properties with experimental data. Comparison of the calculated vibrations of the low-spin Fe(III)OOH confirms the influence of the spin state of iron on the Fe−O and O−O bond strength, proposed in the literature. As the O−O bond strength is decreased and the Fe−O bond strength is increased in the low-spin Fe(III)OOH compared to the high-spin Fe(III)OOH, we expect the reaction free energy barrier for the O−O homolysis to be significantly lower for low-spin complexes.

Acknowledgment. We gratefully acknowledge the helpful discussions with Michiel Gribnau from Unilever in Vlaardingen and the support by the Prioriteits Programma Materialen−Computational Materials Science (PPM-CMS). We thank the foundation NCF of The Netherlands Foundation of Scientific Research (NWO) for computer time.

References and Notes

(1) Fenton, H. J. H. *Chem. News* **1876**, *190*.
(2) Fenton, H. J. H. *J. Chem. Soc.* **1894**, *65*, 899.
(3) Haber, F.; Weiss, J. *Proc. R. Soc. London* **1934**, *147*, 332.
(4) Bray, W. C.; Gorin, M. H. *J. Am. Chem. Soc.* **1932**, *54*, 2124.
(5) Buda, F.; Ensing, B.; Gribnau, M. C. M.; Baerends, E. J. *Chem. Eur. J.* **2001**, *7*, 2775.
(6) Ensing, B.; Buda, F.; Blöchl, P. E.; Baerends, E. J. *Angew. Chem., Int. Ed.* **2001**, *40*, 2893.
(7) Ensing, B.; Buda, F.; Blöchl, P. E.; Baerends, E. J. *Phys. Chem. Chem. Phys.* **2002**, *4*, 3619.
(8) Barb, W. G.; Baxendale, J. H.; George, P.; Hargrave, K. R. *Trans. Faraday. Soc.* **1951**, *47*, 591.
(9) Walling, C.; Weil, T. *Int. J. Chem. Kinet.* **1974**, *6*, 507.
(10) Costas, M.; Chen, K.; Que, L., Jr. *Coord. Chem. Rev.* **2000**, *200*, 517.
(11) Roelfes, G.; Lubben, M.; Hage, R.; Que, L., Jr.; Feringa, B. L. *Chem. Eur. J.* **2000**, *6*, 2152.
(12) Kremer, M. L.; Stein, G. *Trans. Faraday. Soc.* **1959**, *95*, 595.
(13) Ensing, B.; Meijer, E. J.; Blöchl, P. E.; Baerends, E. J. *J. Phys. Chem. A* **2001**, *105*, 3300.
(14) Tuckerman, M.; Laasonen, K.; Sprik, M.; Parrinello, M. *J. Phys. Chem.* **1995**, *99*, 5749.
(15) Geissler, P. L.; Dellago, C.; Chandler, D.; Hutter, J.; Parrinello, M. *Sci.* **2001**, *2121*, 291.
(16) Siegbahn, P. E. M.; Crabtree, R. H. *J. Am. Chem. Soc.* **1997**, *119*, 3103.
(17) Siegbahn, P. E. M. *J. Biol. Inorg. Chem.* **2001**, *6*, 27.
(18) Basch, H.; Mogi, K.; Musaev, D. G.; Morokuma, K. *J. Am. Chem. Soc.* **1999**, *121*, 7249.
(19) Basch, H.; Mogi, K.; Musaev, D. G.; Morokuma, K. *J. Phys. Chem. A* **2001**, *105*, 3615.
(20) Torrent, M.; Musaev, D. G.; Morokuma, K. *J. Phys. Chem. B* **2001**, *105*, 4453.
(21) Dunietz, B. D.; Beachy, M. D.; Cao, Y.; Whittington, D. A.; Lippard, S. J.; Friesner, R. A. *J. Am. Chem. Soc.* **2000**, *122*, 2828.
(22) Harris, D.; Loew, G. H. *J. Am. Chem. Soc.* **1998**, *120*, 8941.
(23) Blomberg, M. R. A.; Siegbahn, P. E. M.; Babcock, G. T.; Wikström, M. *J. Am. Chem. Soc.* **2000**, *122*, 12848.
(24) Siegbahn, P. E. M.; Blomberg, M. R. A. *Chem. Rev.* **2000**, *100*, 421.
(25) Ogliaro, F.; Filatov, M.; Shaik, S. *Eur. J. Inorg. Chem.* **2000**, 2455.
(26) Ogliaro, F.; Harris, N.; Cohen, S.; Filatov, M.; de Visser, S. P.; Shaik, S. *J. Am. Chem. Soc.* **2000**, *122*, 8977.
(27) Yoshizawa, K.; Shiota, Y.; Yamabe, T. *Organometallics* **1998**, *17*, 2825.
(28) Yoshizawa, K.; Shiota, Y.; Yamabe, T. *J. Am. Chem. Soc.* **1998**, *120*, 564.
(29) Yoshizawa, K.; Shiota, Y.; Yamabe, T. *J. Chem. Phys.* **1999**, *111*, 538.
(30) Yoshizawa, K.; Shiota, Y.; Kagawa, Y.; Yamabe, T. *J. Phys. Chem. A* **2000**, *104*, 2552.
(31) Schröder, D.; Schwarz, H.; Shaik, S. *Struct. Bond.* **2000**, *97*, 92.
(32) Shaik, S.; Filatov, M.; Schröder, D.; Schwarz, H. *Chem. Eur. J.* **1998**, *4*, 193.
(33) Filatov, M.; Shaik, S. *J. Phys. Chem. A* **1998**, *102*, 3835.
(34) Parr, R. G.; Yang, W. *Density-Functional Theory of Atoms and Molecules*; Oxford University: New York, 1989.
(35) Baerends, E. J.; Ellis, D. E.; Ros, P. *Chem. Phys.* **1973**, *2*, 41.
(36) Becke, A. D. *J. Chem. Phys.* **1992**, *96*, 2155.
(37) Perdew, J. P. *Phys. Rev. B* **1986**, *33*, 8822.
(38) Chong, D. P. Private communication: high-quality even-tempered all-electron STO basis set.
(39) Car, R.; Parrinello, M. *Phys. Rev. Lett.* **1985**, *55*, 2471.
(40) Blöchl, P. E. *Phys. Rev. B* **1994**, *50*, 17953.
(41) Nosé, S. J. *J. Chem. Phys.* **1984**, *81*, 511.
(42) Halperin, J.; Taube, H. *J. Am. Chem. Soc.* **1952**, *74*, 380.
(43) Flynn, C. M., Jr. *Chem. Rev.* **1984**, *84*, 31.
(44) Baes, C. J.; Mesner, R. E. In *The Hydrolysis of cations*; Krieger, Ed.; Malabar, India, 1986.
(45) Ensing, B.; Baerends, E. J. *J. Phys. Chem. A* **2002**, *106*, 7902.
(46) Ensing, B.; Buda, F.; Baerends, E. J. Manuscript in preparation.
(47) Girerd, J. J.; Banse, F.; Simaan, A. J. *Struct. Bond.* **2000**, *97*, 145.
(48) Ho, R. Y. N.; Roelfes, G.; Hermant, R.; Feringa, B. L.; Que, L., Jr. *J. Am. Chem. Soc.* **1999**, *121*, 264.
(49) Ho, R. Y. N.; Roelfes, G.; Hermant, R.; Hage, R.; Feringa, B. L.; Que, L., Jr. *Chem. Commun.* **1999**, 2161.
(50) Simaan, A. J.; Döpner, S.; Banse, F.; Bourcier, S.; Bouchoux, G.; Boussac, A.; Hildebrandt, G.; Girerd, J. J. *Eur. J. Inorg. Chem.* **2000**, 1627.
(51) Nienhuys, H. K.; van Santen, R. A.; Bakker, H. *J. Chem. Phys.* **2000**, *112*, 8487.
(52) Carter, E. A.; Ciccotti, G.; Hynes, J. T.; Kapral, R. *Chem. Phys. Lett* **1989**, *156*, 472.
(53) den Otter, W. K.; Briels, W. J. *J. Chem. Phys.* **1998**, *109*, 4139.
(54) Chandler, D. *An introduction to modern statistical mechanics*; Oxford University Press: New York, 1987.
(55) Frenkel, D.; Smit, B. *Understanding molecular simulation*; Academic: San Diego, CA, 1996.
(56) Trout, B. L.; Parrinello, M. *Chem. Phys. Lett.* **1998**, *288*, 343.
(57) Tuckerman, M.; Laasonen, K.; Sprik, M.; Parrinello, M. *J. Chem. Phys.* **1995**, *103*, 150.
(58) Neese, F.; Solomon, E. I. *J. Am. Chem. Soc.* **1998**, *120*, 12829.
(59) Ahmad, S.; McCallum, J. D.; Shiemke, A. K.; Appelman, E. H.; Loehr, T. M.; Sanders-Loehr, J. *Inorg. Chem.* **1988**, *27*, 2230.
(60) Shiemke, A. K.; Loehr, T. M.; Sanders-Loehr, J. *J. Am. Chem. Soc.* **1984**, *106*, 4951.